

Thermal Enhancement of Interference Effects in Quantum Point Contacts

Adel Abbout, Gabriel Lemarié, and Jean-Louis Pichard
*Service de Physique de l'État Condensé (CNRS URA 2464),
 IRAMIS/SPEC, CEA Saclay, 91191 Gif-sur-Yvette, France*

We study an electron interferometer formed with a quantum point contact and a scanning probe tip in a two-dimensional electron gas. The images giving the conductance as a function of the tip position exhibit fringes spaced by half the Fermi wavelength. For a contact opened at the edges of a quantized conductance plateau, the fringes are enhanced as the temperature T increases and can persist beyond the thermal length l_T . This unusual effect is explained assuming a simplified model: The fringes are mainly given by a contribution which vanishes when $T \rightarrow 0$ and has a decay characterized by a T -independent scale.

PACS numbers: 85.35.Ds, 07.79.-v, 73.23.-b, 72.10.-d

The quantum circuits used in nanoelectronics are very often built in a two-dimensional electron gas (2DEG) made of a thin sheet of conduction electrons created just beneath the surface of a semiconductor heterostructure. Induced by electrostatic gates deposited at the surface of the heterostructure, the quantum point contact (QPC) is one of the elementary elements of quantum circuits used in a wide variety of investigations, including transport through quantum dots, Mach-Zehnder interferometry and various prototypes of quantum-computing schemes. The quantization [1, 2] in units of $2e^2/h$ of its conductance g can be explained using simple non-interacting models [3–5], outside some anomalies, as the $0.7(2e^2/h)$ anomaly [6], which cannot be explained by a non interacting theory. The recent engineering [7–10]

of the scanning gate microscope (SGM) has allowed to “image” the electron flow associated with the successive conductance plateaus [7, 9] of a QPC. The images are obtained with the charged tip of an AFM cantilever which can be scanned over the surface of the heterostructure. A negatively charged tip causes a depletion region in the 2DEG underneath the tip which scatters the electrons at a distance r from the QPC. The tip and the QPC form an electron interferometer, and the SGM images give its conductance g as a function of the tip position. Fringes falling off with r and spaced by half the Fermi wavelength $\lambda_F/2$ characterize these images.

In mesoscopic physics, the interference effects are usually important when the temperature $T = 0$, and disappear as T increases at scales larger than the thermal length $l_T \propto 1/T$. We discuss here the possibility to observe the opposite behavior, where the interference effects are negligible at $T = 0$, and become important when $T \neq 0$. As recently pointed [11] out, the effect of a charged tip upon g is more important if the QPC is biased outside the conductance plateaus, while the fringes are weaker if the QPC is biased inside a plateau. We show in this letter that the temperature can substantially *enhance* the visibility of the fringes, if the QPC is biased near the ends of a plateau. Moreover, the scale characterizing the decay of the fringes is not l_T , but another length l_T associated with the sharpness of the conductance steps. Fringes persisting above l_T have been seen [8], and the role of impurity scattering was believed to be important for explaining this persisting fringing [14]. Here, we give another mechanism for fringes persisting beyond l_T , valid without impurity scattering, which takes place at the edges of the plateaus and assumes a sharp opening of the QPC conduction channels.

Numerical observations from QPC models: Our observations are based on numerical simulations of QPC models in the ballistic limit where the only source of scattering outside the QPC comes from the depletion region caused by the charged tip. This limit was experimentally studied in Refs. [12, 13]. We have neglected electron-electron interactions acting inside the QPC, though they

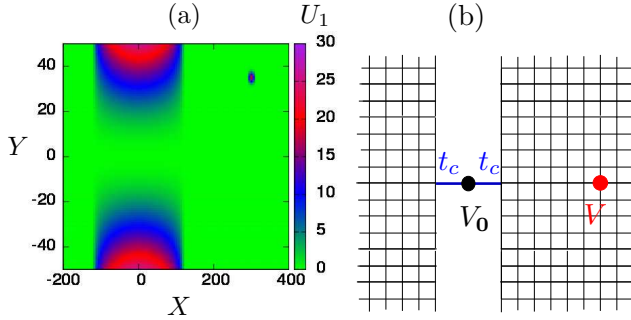


FIG. 1: (color online) Electron interferometer made of a QPC and a scatterer (red point on the right) induced by a charged tip. Fig. (a): Saddle-point QPC potential used in Model 1: $U_1(X, Y) = (Y/L_Y)^2 [1 - 3(X/L_X)^2 + 2|X/L_X|^3]^{1/4}$ for $|X| \leq L_X$ and $U_1 = 0$ elsewhere. $L_Y = 10$ and $L_X = 120$ (i.e. long QPC). Model 2 (hard wall QPC not shown) consists in removing for $|X| \leq L_X$ the sites of coordinates $|Y| \geq L_Y + 3(X/L_X)^2$, with $L_Y = 6$ and $L_X = 20$ but keeping otherwise the site potentials equal to zero. The hopping amplitudes are $t_h = -1$. Fig. (b): Resonant Level Model (RLM): 2 semi-infinite square lattices (with zero on-site potential and hopping amplitudes $t_h = -1$) are contacted by hopping terms t_c via a single site $\mathbf{0}$ of energy V_0 . At a distance x from the contact, there is a tip potential $V \neq 0$.

can change the SGM images of a weakly opened contact [15]. Therefore, our results will exhibit neither the branches [8], nor the $0.7(2e^2/h)$ -anomaly seen in the experiments. We have used lattice models describing an infinite strip, the QPC being defined in a central scattering region. We have taken long adiabatic QPCs for having a sharp opening of the conduction channels [3]. Model 1 consists in a smooth saddle-point contact [4], while model 2 has hard walls [16] (see Fig. 1 and its caption). The effect of the charged tip is modelled by a site-potential $V \neq 0$ at a distance r from the QPC. We have taken small filling factors for being in the continuum limit.

Typical SGM images are shown in Fig. 2 using a QPC biased at the beginning of the first two conductance plateaus. At $T = 0$, the conductance without the tip g_0 is an integer (see the insets which give $g_0(E)$, the arrows indicating the value of E_F) and the interference effects are weak [Figs. 2 (a) and (c)]. However, increasing T enhances the fringes, as shown in Figs. 2 (b) and (d). When $g_0 = 1$, the fringes are in the longitudinal X direction while they have a V shape when $g_0 = 2$. This V shape indicates that the thermal enhancement of the fringes comes only from a contribution of the second conduction channel, and not of the first. In the middle of the plateaus, these angular patterns have been observed in Ref. [7]. A checkerboard pattern of the type discussed in Ref. [13] can be seen in Fig. 2 (b). Last but not least, in Fig. 2 (d), interference fringes can be seen up to $r \approx 4l_T$ (the thermal length $l_T \approx 4\lambda_F/2$): thus we have persistent fringing beyond l_T , a phenomenon which was previously thought to be possible only when there are other scatterers near the tip (see [8, 14]), which is not the case here.

Analytical solution of a Resonant Level Model (RLM): To explain the origin of these temperature induced fringes, we study the simplified interferometer sketched in Fig. 1 (b) where two semi-infinite square lattices with nearest neighbor hopping ($t_h = -1$) are contacted via a single site $\mathbf{0}$ [of coordinate $(0,0)$] with on-site energy V_0 through hopping terms t_c . The effect of the tip is modelled by a potential $V \neq 0$ at the site $(x,0)$ in the right lead. First, we study the zero temperature limit.

When $V = 0$, the Landauer-Büttiker conductance $g_0(E)$ (in units of $2(e^2/h)$) is conveniently expressed in terms of the self-energies $\Sigma_{l,r}(E) = R_{l,r}(E) + iI_{l,r}(E)$ of the left l and right r leads (Fisher-Lee formula [17]):

$$g_0(E) = \frac{4I_l I_r}{(E - V_0 - R_l - R_r)^2 + (I_r + I_l)^2}. \quad (1)$$

$\Sigma_{l,r}(E)$ are related to the retarded Green's functions of the 2 leads evaluated at the 2 sites directly coupled to $\mathbf{0}$: $\Sigma_{l,r}(E) = t_c^2 \langle \pm 1, 0 | G_{l,r}^R(E) | \pm 1, 0 \rangle$. If t_c is small enough, the transmission exhibits a Breit-Wigner resonance of width $\Gamma = -(I_l + I_r)$ at an energy $V_0 + R_l + R_r$. The Green's function $G_{l,r}^R(E, V_T = 0)$ of semi-infinite

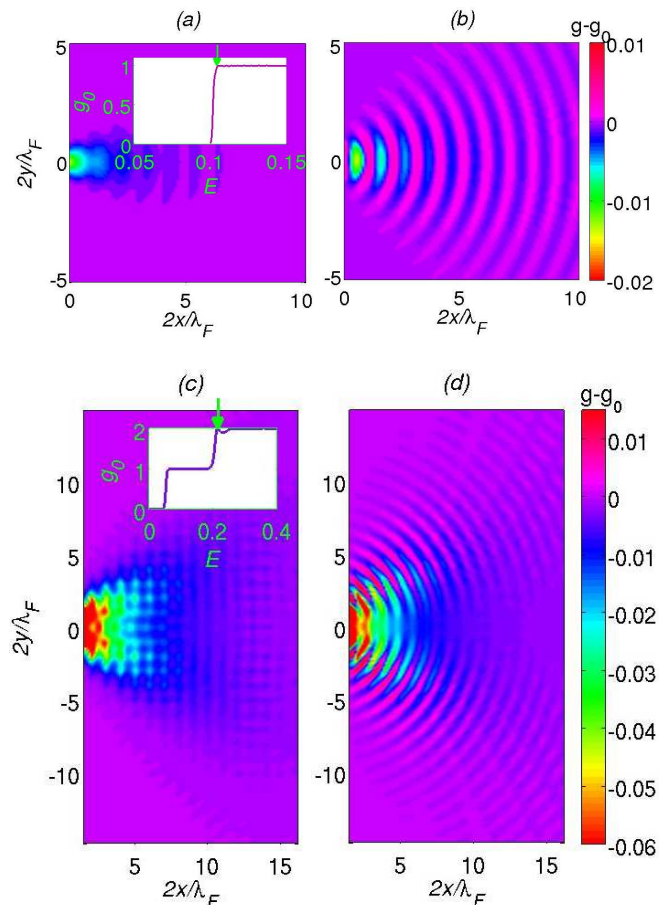


FIG. 2: (color online) $\delta g(T) = g(T) - g_0(T)$ as a function of the tip position (in units of $\lambda_F/2$). The left figures correspond to $T = 0$, while $T \neq 0$ for the right figures. g_0 is biased as indicated by the arrow in the insets (giving $g_0(T = 0)$ as a function of E_F). Figs. 1 (a) and (b): QPC opened at the beginning of the first plateau using model 1 with $V = 1$ and $\lambda_F/2 = 9.65$. $k_B T/E_F = 0.01$ for Fig. 1 (b) ($2l_T/\lambda_F \approx 14.6$). Figs. 1 (c) and (d): QPC opened at the beginning of the second plateau using model 2 with $V = -2$ and $\lambda_F/2 = 6.7$. $k_B T/E_F = 0.035$ for Fig. 1 (c) ($2l_T/\lambda_F \approx 4$).

square lattices can be obtained from the expression valid for an infinite square lattice [18] using the method of mirror images [19].

In the presence of the tip, the conductance $g(E)$ of the QPC-tip interferometer is still given by Eq. (1), if one adds to the self-energy $\Sigma_r(E)$ of the right lead an amount $\Delta\Sigma_r(E)$ which accounts for the effect of the tip. This generalization of the Fisher-Lee formula uses a method introduced in Ref. [20] and will be given in a following paper [21]. Using Dyson's equation, one gets $\Delta\Sigma_r(E) = t_c^2 \rho \exp(i\phi) |\langle 1, 0 | G_r^R | x, 0 \rangle|^2$ where ρ and ϕ are respectively the modulus and the argument of the scattering amplitude $V/(1 - V \langle x, 0 | G_r^R | x, 0 \rangle)$. Hereafter, the x -dependences of ρ and ϕ are neglected, an assumption valid if x is sufficiently large. In the continuum limit

(i.e momentum $k \ll 1$ and energy $E \approx k^2$) and at large distance $kx \gg 1$:

$$\frac{\Delta\Sigma_r(E)}{t_c^2} \approx -\frac{\rho k \exp[i(2kx + \pi/2 + \phi)]}{2\pi x} + O\left(\frac{1}{x^{3/2}}\right). \quad (2)$$

Since $\Delta\Sigma_r(E) \rightarrow 0$ as x increases, the effect $\delta g = g - g_0$ of the tip upon g_0 can be expanded in powers of the reduced variables $\delta R = \Delta R/I$ and $\delta I = \Delta I/I$ (with $I = I_{r,l} \approx -t_c^2 k^2/4$ and $\Delta\Sigma_r = \Delta R + i\Delta I$). The coefficients depend on g_0 and on $S_0 = g_0(1 - g_0)$, the QPC shot noise [22]:

$$\begin{aligned} \delta g = & s g_0 \sqrt{S_0} \delta R + S_0 \delta I + s g_0 \sqrt{S_0} (1 - 2g_0) \delta R \delta I \\ & + g_0^2 \left(\frac{3}{4} - g_0\right) \delta R^2 + g_0^2 \left(-\frac{5}{4} + g_0\right) \delta I^2, \end{aligned} \quad (3)$$

where $s = \text{sign}[(E - V_0 - 2R)/2I]$.

Out of resonance ($g_0 < 1$), the linear terms give a large oscillatory effect of the tip with period $\lambda_F/2$ and $1/x$ -decay:

$$\frac{\delta g}{g_0} \underset{g_0 < 1}{\approx} \frac{2\rho \sin \zeta_0 \cos(2k_F x + \theta)}{\pi k_F x} + O\left(\frac{1}{x^{3/2}}\right), \quad (4)$$

where $\theta \equiv \pi/2 + \phi - \zeta_0$ with $\sin \zeta_0 \equiv s\sqrt{1 - g_0}$. At resonance ($g_0 = 1$), the linear terms vanish and the quadratic terms give a non oscillatory negative correction which falls off as $1/x^2$ accompanied by an oscillatory term δg_{osc} with period $\lambda_F/2$ and $1/x^{5/2}$ -decay:

$$\frac{\delta g}{g_0} \underset{g_0=1}{\approx} -\left(\frac{\rho}{\pi k_F x}\right)^2 - \delta g_{\text{osc}}. \quad (5)$$

This suppression of the linear terms at resonance for the RLM model and the perturbative result derived in Ref. [11] for a QPC yield the same conclusion: interfering electrons are mainly those which contribute to the shot noise S_0 , those of energy around the resonance for the RLM model and those of energy between the plateaus for the QPC.

Let us now consider the temperature dependence of these interferences when E_F is located on the transmission peak ($g_0 = 1$ when $T = 0$). The quantum statistics give an energy scale $\approx k_B T$. The resonant contact gives another energy scale, since it restricts the transmission inside an energy window Γ around E_F . This gives two length scales (over which an electron propagates at the Fermi velocity during the associated time scales) the thermal length $l_T = k_F/(4k_B T \pi^{-1/2})$ yielded by the quantum statistics and the length $l_\Gamma = k_F/\Gamma$ yielded by the resonance. The temperature dependence of the fringes is a function of these two scales. The conductance (in units of $2(e^2/h)$) of the contact at a temperature T reads:

$$g_0(T) = \int_0^\infty g_0(E) \left[-\frac{\partial f_T(E)}{\partial E} \right] dE, \quad (6)$$

the conductance $g_0(E)$ at $T = 0$ characterizing the transmission of an electron of energy E through the contact. The derivative of $f_T(E)$ is approximately given by $-4k_B T \partial f_T(E)/\partial E \approx \exp[-(E - E_F)/(4k_B T \pi^{-1/2})]^2$. The effect of the tip $\delta g(T)$ upon $g_0(T)$ is given by Eq. (6), taking the change $\delta g(E)$ (Eq. (3)) at $T = 0$ instead of $g_0(E)$. At resonance and $T = 0$, $\delta g(x)$ shows only very weak oscillations as x varies (Eq. (5)). If $T \neq 0$, the electrons of non resonant energies E around E_F enhance the interference effects via their linear ρ/x contributions in the expansion (3), which become non zero when $S_0(E) \neq 0$. However, the thermal enhancement of the fringes at short distances vanishes at long distances, since the fast oscillations of the linear terms as E varies destroy the interferences when $kx \gg 1$. To check this quantitatively, one must calculate the integral over energy explicitly. Doing standard approximations (see Ref. [23]), we get:

$$\frac{\delta g(T)}{g_0(T)} \approx A \left(\frac{x}{l_\Gamma}, \frac{l_T}{l_\Gamma} \right) \frac{\rho \cos(2k_F x + \phi)}{2\pi k_F x} - \frac{\rho^2}{(\pi k_F x)^2}. \quad (7)$$

The amplitude A (shown in Fig. 3 (b)) is given by

$$A(\mu, \nu) = \frac{(1 + 2\mu + 4\nu^2)F_+ + F_- - G}{\text{erfc}(\nu)}, \quad (8)$$

where $F_\pm = e^{\pm\mu} \text{erfc}\left[\frac{2\nu^2 \pm \mu}{2\nu}\right]$ and $G = \frac{4\nu}{\sqrt{\pi}} e^{-\nu^2 - \frac{\mu^2}{4\nu^2}}$. Three main results can be seen: (i) A vanishes when $T \rightarrow 0$, i.e. when $l_T \gg l_\Gamma$; (ii) When $x \gg l_T$, there is a universal asymptotic $\exp(-x/l_\Gamma)$ -decay characterized by the T -independent scale l_Γ , and not by l_T ; (iii) A has a maximum when $x \approx l_T$. Fig. 3 (a) shows a comparison between the analytical formula (7) and the results of numerical simulations of the RLM. The agreement is very good, without any adjustable parameter.

For the RLM model, $g_0(E)$ is given by a Lorentzian and $g_0 = 1$ only at resonance. For a QPC, $g_0(E)$ is a step-like function where $g_0 = 1$ over the first plateau. For extending the results of the RLM model to a QPC with $g_0 \leq 1$, we summarize the arguments which will be given in a following paper [21]. Firstly, we have checked that the expansion (3) describes also (up to a phase factor) the effect of a tip upon a QPC when $g_0 \leq 1$, if one uses in Eq. (3) the step-like function $g_0(E)$ of the QPC instead of the Lorentzian $g_0(E)$ of the RLM model. Secondly, the linear terms in Eq. (3) depend on $g_0(E)$ through the combination $g_0(E)[1 - g_0(E)]$ which characterizes the QPC shot noise. For a QPC, the scale Γ is thus given by the energy scale over which the QPC shot noise (and not the QPC transmission) is important. If $l_\Gamma \gg l_T$, persistent fringing beyond l_T can be observed even without impurity scattering.

In summary, the SGM fringes observed at low temperatures using a QPC biased near the ends of a conductance plateau are mainly due to a thermal effect which vanishes

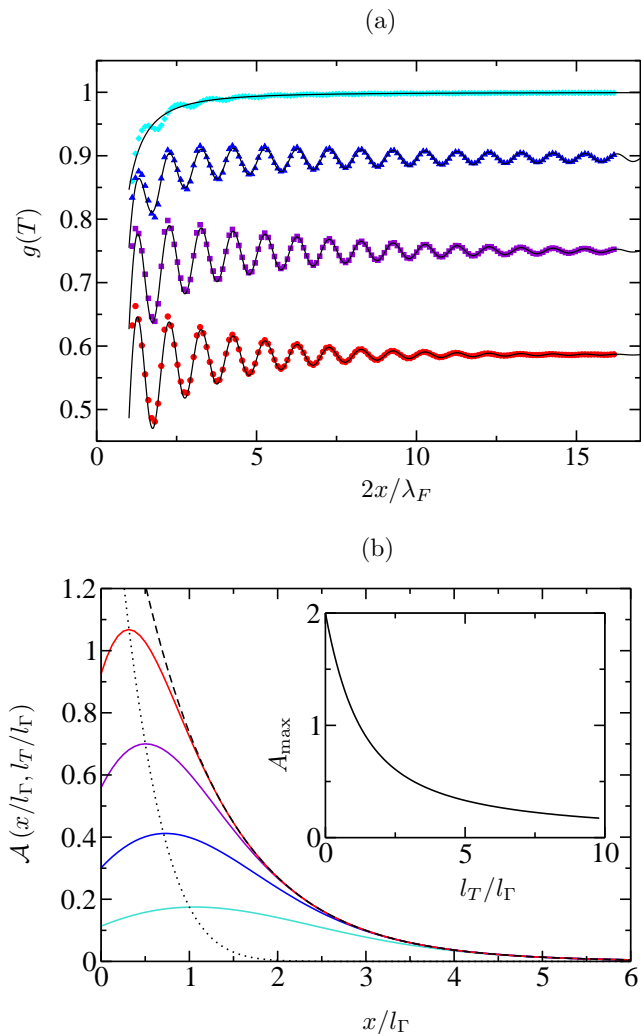


FIG. 3: (Color online) (a) RLM conductance $g(T)$ as a function of $2x/\lambda_F$ for increasing temperatures (from top to bottom). The color points are results obtained by direct numerical simulations, taking from top to bottom $2l_T/\lambda_F = \infty$, 8.8, 4.4 and 2.2. The solid lines give the analytical results (Eq. (7)). $t_c = 0.4$, $V = -2$, $\lambda_F/2 \approx 10$ and $2l_T/\lambda_F \approx 4$. (b) As a function of x/l_T , rescaled amplitude $\mathcal{A} = A(x/l_T, l_T/l_T) \operatorname{erfc}(l_T/l_T)$ for fixed l_T and increasing temperatures, i.e. ratios $l_T/l_T = 1$ (light blue), 0.7 (blue), 0.5 (violet) and 0.3 (red) (solid lines from bottom to top). The dashed and dotted lines give respectively the asymptotic behavior $2\exp(-x/l_T)$ valid for $x \gg l_T$ and the function $\mathcal{A}(l_T/l_T, l_T/l_T)$ where \mathcal{A} is maximum. Inset: maximum A_{\max} of the bare amplitude A as a function of l_T/l_T .

when $T \rightarrow 0$ and decays with a T -independent length l_T . More generally, the thermal enhancement and the persistence beyond l_T of interference effects can be observed if one uses electron interferometers made of two scatterers, one of them having a resonance at E_F . Fermi-Dirac statistics give rise to a temperature induced interferometer which disappears as $T \rightarrow 0$ if one of the scatterers

is transparent at E_F and is only seen by the electrons of energy $E \neq E_F$. Moreover, the resonant scatterer acts as a filter, yielding interferences over a scale independent of the temperature (a somewhat related phenomenon has been observed in Ref [24]). Studying the SGM images, we have shown that a QPC also can filter the interfering electrons as does a resonant scatterer, allowing better quantum interference effects.

We thank A. Freyn, R. A. Jalabert, K. A. Muttalib, F. Portier and D. Weinmann for useful discussions, and the French National Agency ANR (project ANR-08-BLAN-0030-02 ‘‘Item-Th’’) for financial support.

-
- [1] B. J. van Wees *et al.*, Phys. Rev. Lett. **60**, 848 (1988).
 - [2] D. Wharam *et al.*, J. Phys. C **21**, L209 (1988).
 - [3] L. Glazman, G. Lesovik, D. Kmelnitskii, and R. Shekhter, JETP Lett. **48**, 238 (1988).
 - [4] M. Büttiker, Phys. Rev. B **41**, 7906 (1990).
 - [5] C. W. J. Beenakker and H. Van Houten, Solid State Physics **44**, 1 (1991), URL arXiv:cond-mat/0412664v1.
 - [6] K. J. Thomas *et al.*, Phys. Rev. Lett. **77**, 135 (1996).
 - [7] M. Topinka, B. LeRoy, S. Shaw, E. Heller, R. Westervelt, K. Maranowski, and A. Gossard, Science **289**, 2323 (2000).
 - [8] M. Topinka, B. LeRoy, R. Westervelt, S. Shaw, R. Fleischmann, E. Heller, K. Maranowski, and A. Gossard, Nature **410**, 183 (2001).
 - [9] M. Topinka, R. Westervelt, and E. Heller, Physics Today **56**, 47 (2003).
 - [10] B. J. LeRoy *et al.*, Phys. Rev. Lett. **94**, 126801 (2005).
 - [11] R. A. Jalabert, W. Szewc, S. Tomsovic, and D. Weinmann, Phys. Rev. Lett. **105**, 166802 (2010).
 - [12] M. P. Jura *et al.*, Nat. Phys. **3**, 841 (2007).
 - [13] M. P. Jura, M. A. Topinka, M. Grobis, L. N. Pfeiffer, K. W. West, and D. Goldhaber-Gordon, Phys. Rev. B **80**, 041303 (2009).
 - [14] E. Heller, K. Aidala, B. LeRoy, A. Bleszynski, A. Kalben, R. Westervelt, K. Maranowski, and A. Gossard, Nano Lett. **5**, 1285 (2005).
 - [15] A. Freyn, I. Kleftogiannis, and J.-L. Pichard, Phys. Rev. Lett. **100**, 226802 (2008).
 - [16] A. Szafer and A. D. Stone, Phys. Rev. Lett. **62**, 300 (1989).
 - [17] S. Datta, *Electronic transport in mesoscopic systems* (Cambridge Univ Pr, 1997).
 - [18] E. Economou, *Green’s functions in quantum physics* (Springer Verlag, 2006).
 - [19] M. I. Molina, Phys. Rev. B **74**, 045412 (2006).
 - [20] P. Darancet, V. Olevano, and D. Mayou, Phys. Rev. B **81**, 155422 (2010).
 - [21] G. Lemarié, A. Abbout, and J.-L. Pichard, in preparation.
 - [22] C. W. J. Beenakker and C. Schönberger, Physics Today p. 37 (May 2003).
 - [23] F. Mezei and G. Grüner, Phys. Rev. Lett. **29**, 1465 (1972).
 - [24] N. C. van der Vaart *et al.*, Phys. Rev. Lett. **74**, 4702 (1995).